frontiers in Materials

ORIGINAL RESEARCH
published: 19 February 2020
doi: 10.3389/fmats.2020.00034

Crystallization of the $Na_2Fe_xNi_{1-x}P_2O_7$ Glass and Ability of Cathode for Sodium-Ion Batteries

Yongzheng Ji, Tsuyoshi Honma and Takayuki Komatsu*

Department of Materials Science and Technology, Nagaoka University of Technology, Nagaoka, Japan

Although the sodium phosphate cathode active materials based on the Ni^{3+}/Ni^{2+} redox reaction are expected to develop a high discharge potential, none of the studies aimed at practical application have been reported due to its poor kinetics showed in the sodium phosphate. Herein, we substituted active Fe for a part of Ni, expecting to activate the potential deriving from the $Ni^{3+/2+}$ in $Na_2Fe_xNi_{1-x}P_2O_7$ glass-ceramics. Precursor glasses were prepared by the melt-quenching method and exhibited surface crystallization tendency due to heterogeneous nucleation. In the charge-discharge testing, all the flat potential showed in the discharge process derived from the reduction of $Fe^{3+/2+}$. However, from the dQ/dV plot, there were two weak reduction peaks at 4.3 and 4.4 V in the discharge process of $Na_2Fe_{0.25}Ni_{0.75}P_2O_7$. Combining with the oxidation peak at 4.6 V in the second charge process of $Na_2NiP_2O_7$, we believe the reduction peaks at 4.3 and 4.4 V were derived from the $Ni^{3+/2+}$.

Keywords: glass-ceramics, crystallization behavior, sodium-ion batteries, cathode materials, charge-discharge test

OPEN ACCESS

Edited by:
Ashutosh Goel,
Rutgers, The State University of New Jersey, United States

Reviewed by:
Shi-Xi Zhao,
Graduate School at Shenzhen, Tsinghua University, China
Balaji Rao Ravuri,
Gandhi Institute of Technology and Management (GITAM), India

****Correspondence:***
Tsuyoshi Honma
honma@mst.nagaokaut.ac.jp

Specialty section:
This article was submitted to Glass Science, a section of the journal Frontiers in Materials

Received: *30 September 2019*
Accepted: *30 January 2020*
Published: *19 February 2020*

Citation:
Ji Y, Honma T and Komatsu T (2020) Crystallization of the $Na_2Fe_xNi_{1-x}P_2O_7$ Glass and Ability of Cathode for Sodium-Ion Batteries. Front. Mater. 7:34. doi: 10.3389/fmats.2020.00034

INTRODUCTION

At present, Lithium-Ion Rechargeable Batteries (LIBs) are widely applied to small electronic equipment such as mobile phones and laptop computers, due to the high voltage, high energy density, and long charge-discharge cycle life (Nishi, 2001; Nitta et al., 2015). However, high cost and low safety (Spotnitz and Franklin, 2003; Wang et al., 2012; Finegan et al., 2015) are becoming enormous challenges for them. On the other hand, accompanied by the development of science and technology, drastic improvement of the energy and power density is required, so developing new electrode materials is necessary.

Considering the abundance of sodium ions existing (Slater et al., 2013) and the nearest ion radius with lithium-ion in the group of alkali metal elements in the periodic table, quantities of researchers paid their attention to sodium rechargeable batteries. As a matter of fact, due to the dense atomic mass and larger ionic radius, SIBs commonly generate a lower energy density (Kundu et al., 2015) and a shorter cycle life (Ong et al., 2011) than LIBs. Therefore, the object of these problems is the most critical challenge for SIBs. Some researchers focus on cathode materials to promote the storage of sodium ions. There are numerous types of cathode materials for SIBs had been reported, such as transition-metal layered oxides Na_xMO_2 (Yabuuchi et al., 2012; Wang et al., 2016), Phosphates $NaMPO_4$ (Fang et al., 2015; Bianchini et al., 2018), Pyrophosphates $Na_2MP_2O_7$ (Honma et al., 2012, 2013; Barpanda et al., 2013b), Fluorophosphates Na_2MPO_4F

(Ellis et al., 2010), Sulfates $Na_2M_2(SO_4)_3$ (Barpanda et al., 2014) and $NaM(SO_4)_2$ (Singh et al., 2015). In addition to exploiting the cathode materials, synthesis should be low-cost. Crystallization of glasses is a simple method, which starting from the low-cost precursor glasses for the fabrication of crystalline materials with desired shapes and functions (Komatsu, 2015; Deubener et al., 2018). Glass-forming oxide P_2O_5 makes this an excellent method to synthesis Phosphates and Pyrophosphates. We have investigated and analyzed the crystallization and electrical performance of some active materials in LIBs or SIBs based on the glass or glass-ceramics (Nagamine et al., 2011, 2012; Honma et al., 2012).

$Na_2FeP_2O_7$ has been acknowledged that it could be the cathode candidate for the rechargeable sodium-ion second batteries (SIBs). Among the reports about the electrochemical properties of $Na_2FeP_2O_7$, it exhibited a high potential of 2.9 V and a high discharge capacity of 88 mAh/g, which is 90% of the theoretical capacity based on the glass-ceramics (Honma et al., 2012). Owing to the high thermal stability (Barpanda et al., 2013a) and excellent properties exhibited by the electrochemical charge-discharge testing (Kim et al., 2013), it is looked forward to being used as the positive material in SIBs to instead of LIBs. Besides, Yamauchi demonstrated an oxide all-solid-state battery that positively utilizes the viscous flow of the $Na_2FeP_2O_7$ precursor glass and a glass-ceramics (Yamauchi et al., 2019). According to the Crystal field splitting of the M^{2+} cations in octahedral coordination, it indicated that the Ni^{2+} delivered the highest potential in the lithium or sodium system (Gutierrez et al., 2013). Hence the Ni^{2+} based on the stable three-dimensional framework composed of $(P_2O_7)^{4-}$ with Na ions is expected to exhibit a higher potential than that of Fe^{2+}. Unfortunately, $Na_2NiP_2O_7$ was reported that Ni was not active in the pyrophosphate framework under the electric test (Zhang et al., 2017).

Furthermore, a similar result was also obtained in $Na_2MnP_2O_7$ glass-ceramics with none activity of Mn^{2+} (Tanabe et al., 2018). However, in the $Na_2Fe_{0.25}Mn_{0.75}P_2O_7$ compound with a little Fe substitution, it appeared a high potential of 3.8 V derived from $Mn^{3+/2+}$ (Tanabe et al., 2018). Therefore, the appearance of $Ni^{3+/2+}$ in higher potential with Fe substitution is expected. In this study, the crystallization behavior, density, and electrochemical properties of $Na_2Fe_xNi_{1-x}P_2O_7$ glass or glass-ceramics will be reported for the first time.

EXPERIMENTS

The precursor $Na_2Fe_xNi_{1-x}P_2O_7$ glasses (x = 1, 0.75, 0.5, 0.25, 0) were prepared by melt-quenching method. Under the composition of $33.3Na_2O$-33.3xFeO-33.3 (1−x) NiO-$33.3P_2O_5$ (mol%), the precursor chemicals sodium dihydrogen phosphate (98.0% NaH_2PO_4, Nakarai Tesque Co., Japan), iron mono-oxide (99.5% FeO, Kojyundo Chemicals Co., Japan) and nickel mono-oxide (99.9% NiO, Kojundo Chemicals Co., Japan) were weighted and mixed. Then the mixed $Na_2NiP_2O_7$ powder was melted in a platinum crucible at 1,200°C for 30 min in the air atmosphere, and other composition powder was melted in a graphite crucible at 1,200°C for 30 min in the nitrogen atmosphere by an electric furnace. The melt was then poured onto a steel plate and quenched with another steel plate to produce a bulk glass precursor.

In order to confirm the amorphous state and identify the crystalline phase, the X-ray diffraction (XRD) was performed on Rigaku Ultima IV X-ray diffractometer (Rigaku, Japan) equipped with Cu-Ka radiation (40 kV, 40 mA, and λ = 0.154056 nm) in a speed of 5 deg./min between 10 and 70 deg. The density of the samples was determined by using the XS205 Dual Range analytical balance (METTLER TOLEDO, Japan) by the Archimedes principle. Differential thermal analysis (DTA, Thermoplus EVO TG-8120, RIGAKU Corp., Japan) was used to determine the glass transition temperature T_g, glass crystallization onset temperature (T_x), and glass crystallization temperature T_p of the samples. All the processes performed under the N_2 atmosphere, and the temperature scanning rate of 10 K min^{-1}. Scanning Electron Microscope (SEM, KEYENECE VE-8800) was used to check the crystallization behavior of the glasses.

Because of the strong covalent bond in the pyrophosphates could lead to a low electric conductivity, so the carbon coating was necessary (Chung et al., 2002). An automatic mortar ground the glass precursors for 30 min and selected by a sieve in which the particle size was under or equaled 105 μm. And then, the mixture composed of glass precursors and carbon black (CB) in a weight ratio of 84.2: 15.8 placed into a ZrO_2 pot (45 cm^3) together with 50 g balls (3 mm) and 10 ml methanol, so the mixture would be mixed and pulverized for 15 min × 4 cycles in 700 rpm by wet ball-milling (FRITSCH Premium line P7). After wet ball-milling, we used an evaporator (Tokyo Rika Kikai, N-1110V) to distill off the rudimental methanol and dried the mixture (glass/CB)

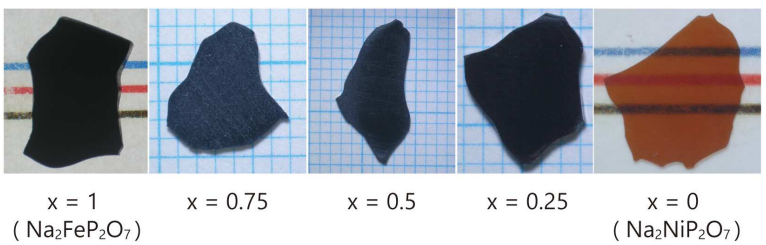

FIGURE 1 | Appearance of the fabricated $Na_2Fe_xNi_{1-x}P_2O_7$ glasses.

at 80°C for 1 h. In order to fabricate the positive electrode materials, we did a heat-treatment regarding the mixture of $Na_2Fe_xNi_{1-x}P_2O_7$ glass and CB. Heat-treatment was performed on glass crystallization temperature T_p for 3 h under a nitrogen atmosphere. We used Polyvinylidene fluoride (PVDF) as a binder with the mixture of crystallized $Na_2Fe_xNi_{1-x}P_2O_7$ glass-ceramics and graphite in a weight ratio 5:95 in a mortar. In order to prepare a slurry to coat on the aluminum foil, we dropped a little N-methylpyrrolidone (NMP) as a solvent to mix with that and dried the coated Al foil at 80°C for 1 h. Finally, the positive electrode was punched out as 16 mmϕ and dried at 100°C in a vacuum oven all night. Sodium metal foils were used as the negative electrodes, the glass filter papers (Advantec Co., GA-100) were used as a separator, and the solution of 1 M $NaPF_6$ in a mixture of ethylene carbonate (EC) and diethyl carbonate (DEC) (1:1, v/v) was used as the electrolyte. The test cells were assembled by the flat cells in an argon-filled glove box, in which the dew point temperature kept at −86°C. The charge-discharge test was performed at a cutoff voltage of 1.5–4.9 V and a rate of 1/10 C by a battery testing system (Hokuto-denko Co.).

The theoretical capacity and corresponding electrochemical reaction formula is showing below:

$$\text{Theoretical capacity (mAh/g)} = \frac{n\ (\text{mol}) \times F\ (\text{C/mol})}{M\ (\text{g/mol}) \times 3600\ (\text{s/h})} \times 1000\ (\text{mA/A})$$

n is the theoretical mole number of the de-insertion sodium ions; F is the Faraday constant; M is the mole mass of the cathode material.

The electrical resistance of glass-ceramics was measured in the form of a pellet with a thickness of 1.0 mm by an alternating current (AC) impedance method (HIOKI 3522-50 LCR Hi-TESTER, Japan) with the electrode diameter of 6.0 mmϕ in the frequency range of 4–100 kHz.

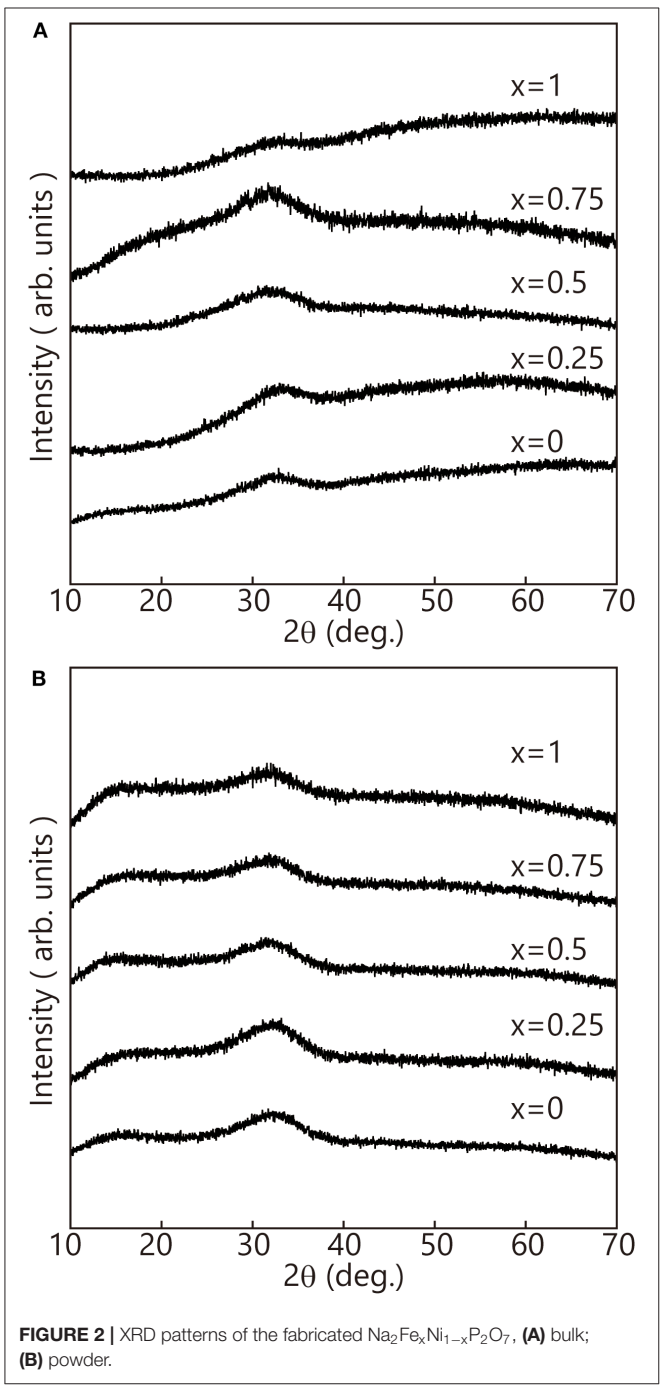

FIGURE 2 | XRD patterns of the fabricated $Na_2Fe_xNi_{1-x}P_2O_7$, **(A)** bulk; **(B)** powder.

RESULTS AND DISCUSSION

Amorphous State

Figure 1 shows the appearance of the fabricated precursor glasses. $Na_2NiP_2O_7$ showed a rust-red color and high

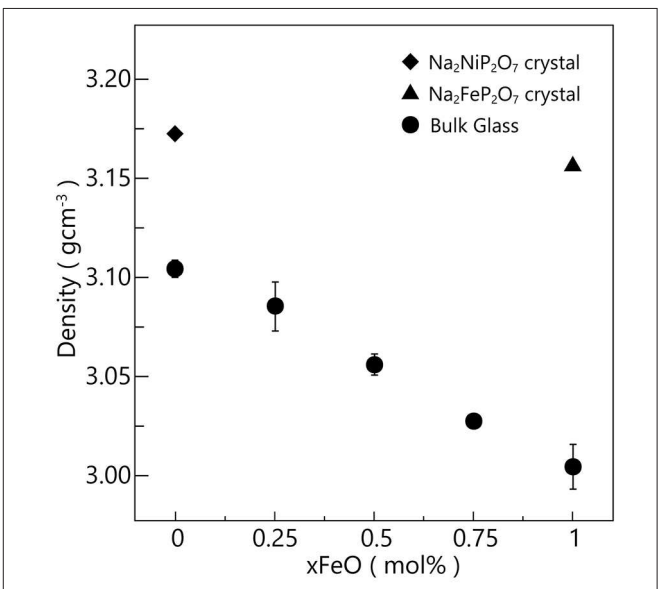

FIGURE 3 | Density of the fabricated $Na_2Fe_xNi_{1-x}P_2O_7$ glass and $Na_2MP_2O_7$ (M = Ni, Fe) crystal.

transparency. However, the other samples showed a black color, and only the $Na_2Fe_{0.25}Ni_{0.75}P_2O_7$ exhibited low transparency. XRD patterns of the bulk and powder, which was pulverized from bulk by an agate mortar of the obtained samples, are shown in **Figure 2**. All samples showed the typical halo patterns of amorphous with no crystallization.

Density Measurement

Figure 3 shows the density result of the fabricated glasses. So we can see that as the x (FeO content) increasing, the density of the glasses tends to be decreasing as a straight line, owing to the molecular weight of FeO is smaller than that of NiO. **Figure 3** also shows the calculated theoretical density of the $Na_2MP_2O_7$ (M = Ni, Fe) crystal in **Figure 3**. So we can see that the density of $Na_2NiP_2O_7$ glass is about 97.9% of $Na_2NiP_2O_7$ crystal, and the density of $Na_2FeP_2O_7$ glass is about 95.2% of $Na_2FeP_2O_7$ crystal. The two unparallel lines of the glass and crystal densities changes indicated that there was a little part of oxidized Fe^{3+} existed in the glass. Because Fe^{3+} ions are more natural to form tetrahedral configuration, so the real density of $Na_2FeP_2O_7$ glass is smaller than the theoretical value with all Fe^{2+} hexahedral configuration. By the way, for the existing of Fe^{3+}, the glasses were fabricated easier, and the network of the glasses will be more stable. Such behavior can be confirmed in the process of glass fabrication (Hirose et al., 2008; Honma et al., 2010).

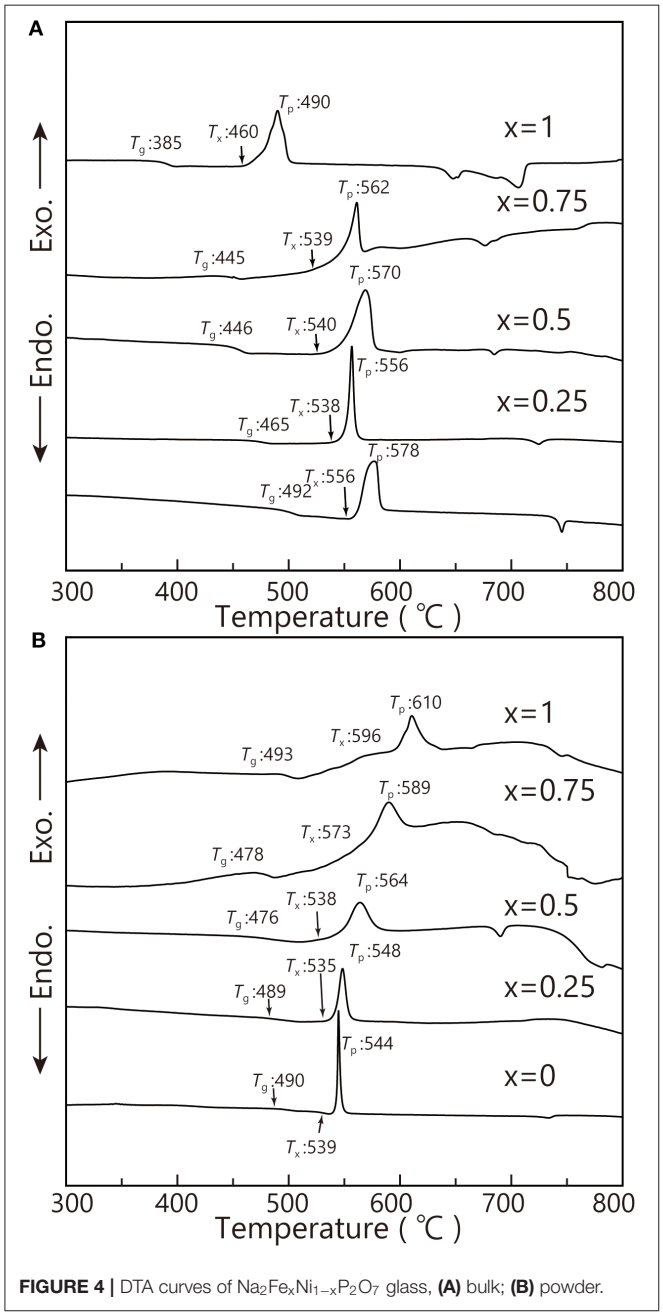

FIGURE 4 | DTA curves of $Na_2Fe_xNi_{1-x}P_2O_7$ glass, **(A)** bulk; **(B)** powder.

Crystallization Mechanism

Figure 4 shows the DTA curves of bulk and powder of the obtained samples. The endothermic dips suggest the glass transition temperature (T_g), and the exothermic peaks suggest the glass crystallization temperature (T_p). The crystallization onset temperature (T_x) is also shown in **Figure 4**. However, we can see that there is a considerable crystallization behavior difference between bulk and powder of $Na_2FeP_2O_7$ from the DTA results. Because the shape of the DTA pattern is sensitive to the oxidized surface area of the bulk and powder, the T_g and T_x of the glass powder are much higher than those of the bulk glass.

The heat-treatment temperature was depended on the glass crystallization temperature (T_p) of the powder, so the heat-treatment was performed on 544, 548, 564, 589, and 610°C. The XRD patterns of that are shown in **Figure 5**. $Na_{3.12}Fe_{2.44}(P_2O_7)_2$ (Angenault et al., 1995) crystal was obtained from the $Na_2FeP_2O_7$ and $Na_{3.14}Ni_{2.18}(P_2O_7)_2$ crystal (Erragh et al., 2000) was obtained

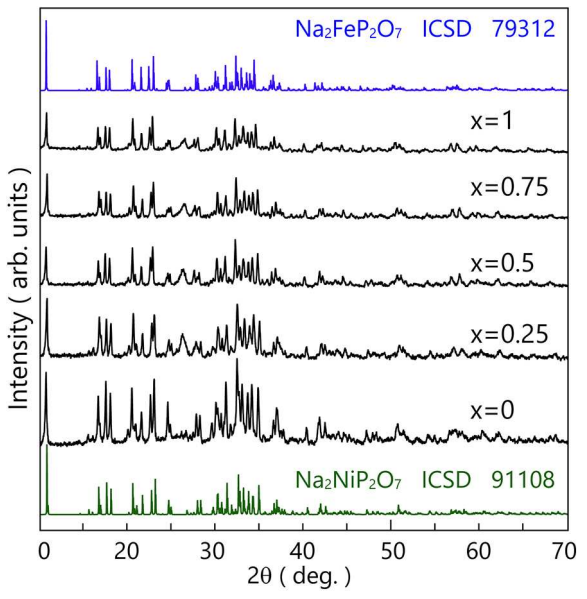

FIGURE 5 | XRD patterns of heat-treated $Na_2Fe_xNi_{1-x}P_2O_7$ glass-ceramics with CB.

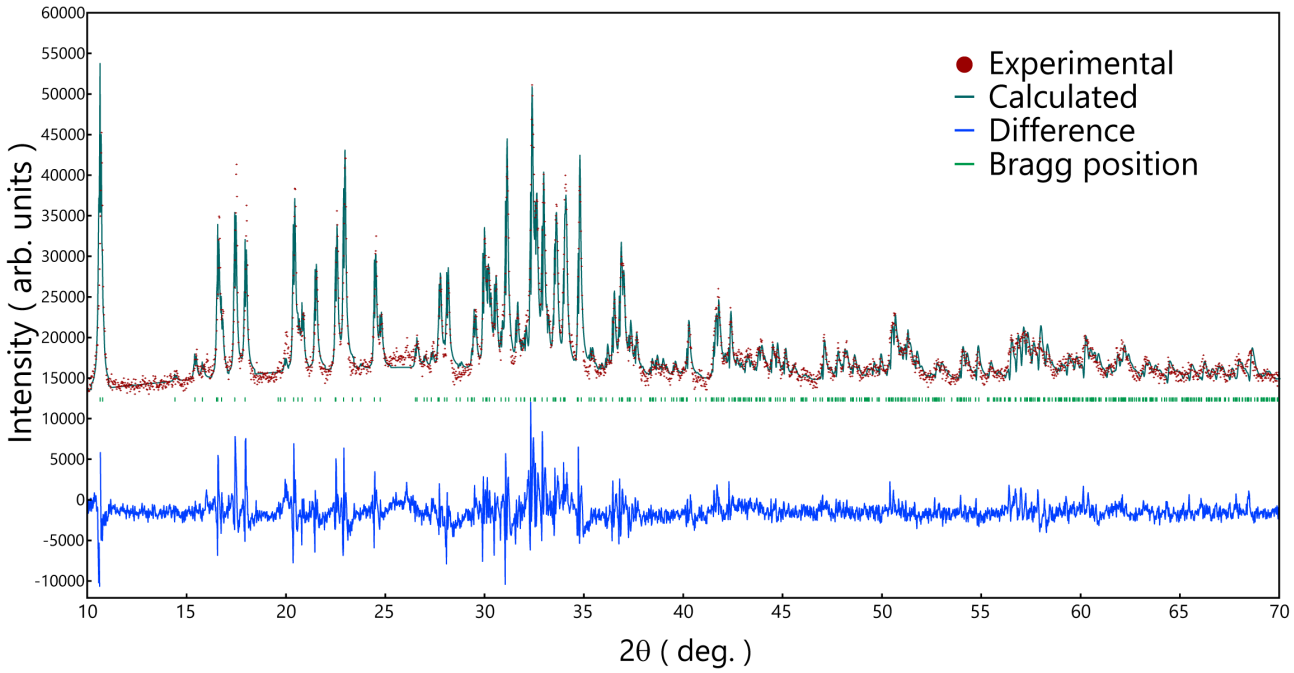

FIGURE 6 | XRD pattern and Rietveld refinement for the mixture of heat-treated $Na_2NiP_2O_7$ and CB.

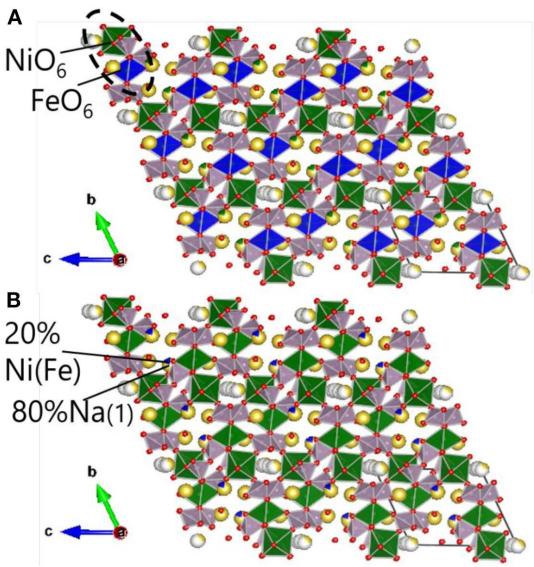

FIGURE 7 | Crystal structure of $Na_2Fe_xNi_{1-x}P_2O_7$, **(A)** Ni-Fe substitution type 1; **(B)** Ni-Fe substitution type 2. Na (yellow), Fe (blue), Ni (green), P (purple), O (red).

from the other composition of $Na_2Fe_xNi_{1-x}P_2O_7$ ($x = 0.75$, 0.5, 0.25, and 0). The simulated patterns of the two kinds of crystals are also shown in **Figure 5**, which with no other crystal phase precipitated.

In order to analyze the $Na_2NiP_2O_7$ crystalline phase in the mixture of $Na_2NiP_2O_7$ glass-ceramics and CB, Rietveld refinement on the powder XRD pattern was performed, and the result is shown in **Figure 6**. According to the $Na_{3.14}Ni_{2.18}(P_2O_7)_2$ crystal structure, which is shown in **Figure 7**, the group of PO_4(tetrahedral), NiO_6(octahedral), and FeO_6(octahedral) units combine by corner-sharing to provide a stable three-dimensional framework to support the de-insertion along the (100) direction of sodium ions. Two types of Ni-Fe substitution were discussed, basing on the position of the Ni atoms. The image of type 1 is shown in **Figure 7A**, which suggests that the Ni-Fe substitution occurred in the NiO_6 units. Besides, the image of type 2 is shown in **Figure 7B**. It suggests that Fe substituted a part of Ni in the Na (1) sites, which contained about 80% Na and 20% Ni. Owing to the two kinds of substitution type could not be decided which one was main, so lattice parameters were analyzed out by Rietveld refinement.

We summarized the lattice parameters of the crystalline phase as shown in **Table 1**. It also shows clearly in **Figure 8** that with the Fe substitution increasing, *a*, *b*, *c* axes, and volume were going up at the same time. However, alpha, beta, gamma did not exhibit any component dependency. Because the ionic radius of Fe^{2+} is larger than that of Ni^{2+}, so the Ni-Fe substitution existed in the $Na_2NiP_2O_7$ crystal. Since the Ni-Fe substitution type 1 has a significant influence on the crystal structure, it could be the primary way of Ni-Fe substitution. When the lattice parameters (*a*, *b*, *c*) increased by Ni-Fe substitution, the crystal volume got larger than before, and it will be advantaged for the de-insertion of sodium ions.

We did the heat-treatment between T_g and T_x on the $Na_2FeP_2O_7$ and $Na_2NiP_2O_7$ bulk glasses and observed the crystallization behavior by SEM. **Figure 9** shows the SEM images of a fracture surface of the samples crystallized by heat

TABLE 1 | Lattice parameters of crystallized $Na_2Fe_xNi_{1-x}P_2O_7$ glass-ceramics.

Composition *x*	*a* (Å)	*b* (Å)	*c* (Å)	Alpha (deg.)	Beta (deg.)	Gamma (deg.)	Volume (Å^3)
1	6.451	9.444	11.047	64.384	85.426	72.796	578.812
0.75	6.430	9.428	11.027	64.311	85.336	72.934	575.053
0.5	6.411	9.417	11.007	64.259	85.270	73.047	571.766
0.25	6.388	9.396	10.959	64.313	85.378	73.242	566.912
0	6.376	9.397	10.911	64.489	85.746	73.508	564.874

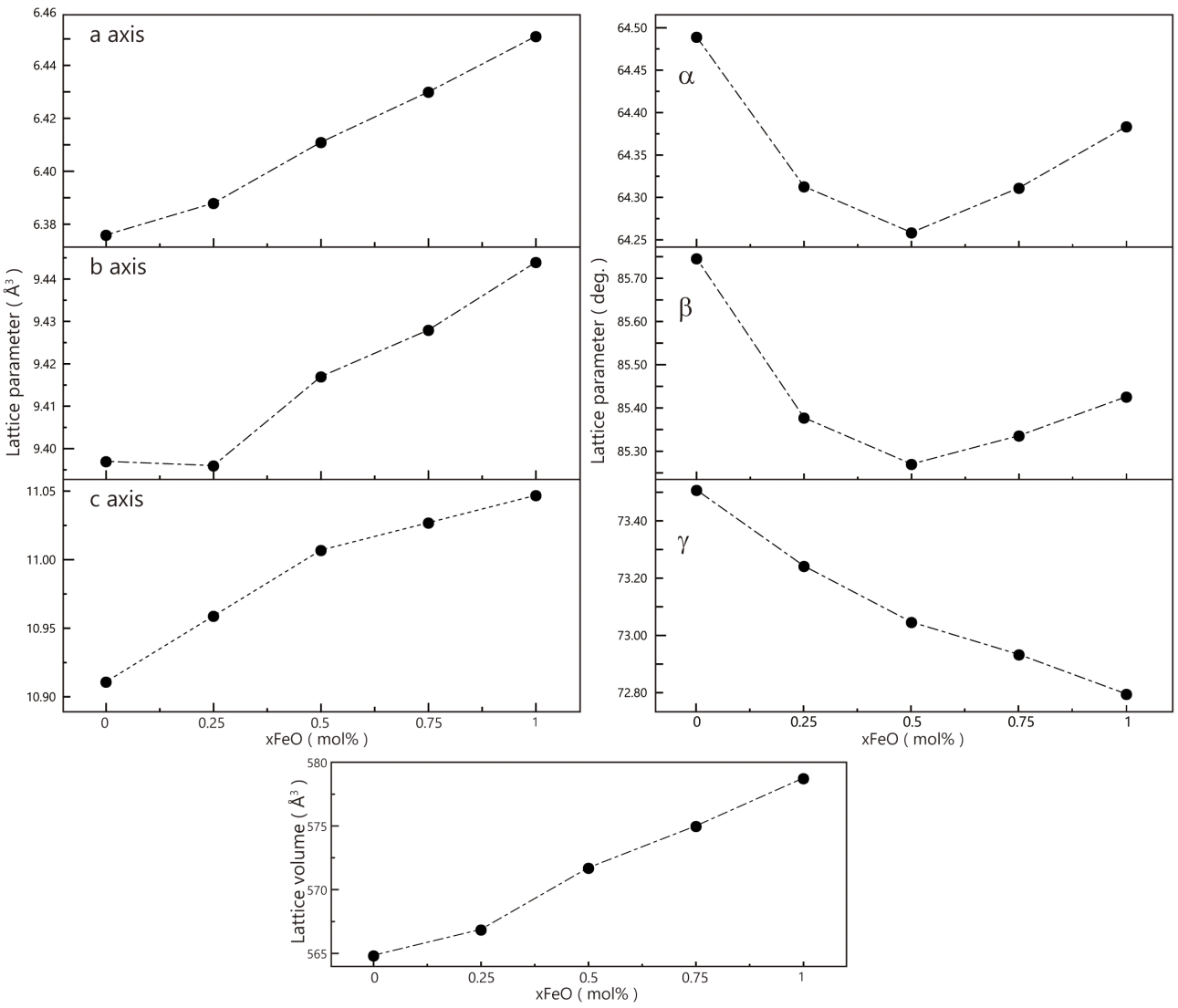

FIGURE 8 | Lattice parameters of crystallized $Na_2Fe_xNi_{1-x}P_2O_7$ glass-ceramics.

treatment. The same crystallization behavior can be observed that both $Na_2FeP_2O_7$ and $Na_2NiP_2O_7$ bulk glasses prefer to develop the crystalline phase on the glass surface. Surface crystallization can lead to high crystal orientation, so such outstanding crystallization behavior is expected to improve the ionic conduction of cathode materials (Akatsuka et al., 2018). Another aspect, the $Na_2NiP_2O_7$ glass exhibits thermal instability because the ΔT ($T_{\text{heat-treatment}} - T_g$) is only 8°C. Hence, we obtained more thick surface crystallied architecture in $Na_2NiP_2O_7$ rather than $Na_2FeP_2O_7$.

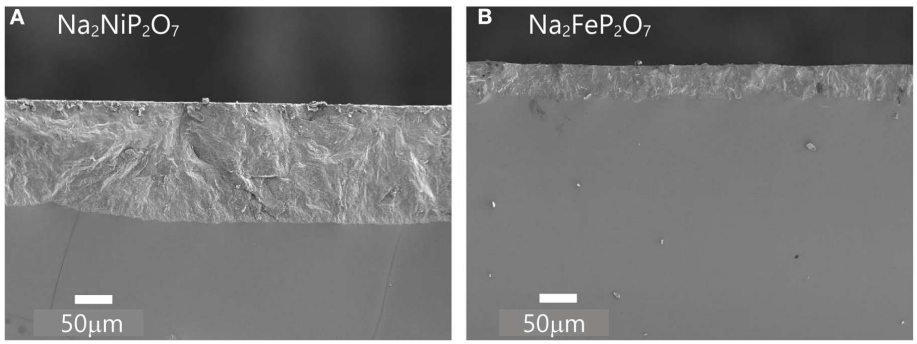

FIGURE 9 | The section SEM image of **(A)** $Na_2NiP_2O_7$ heat-treated at 500°C for 3 h; **(B)** $Na_2FeP_2O_7$ heat-treated at 430°C for 3 h.

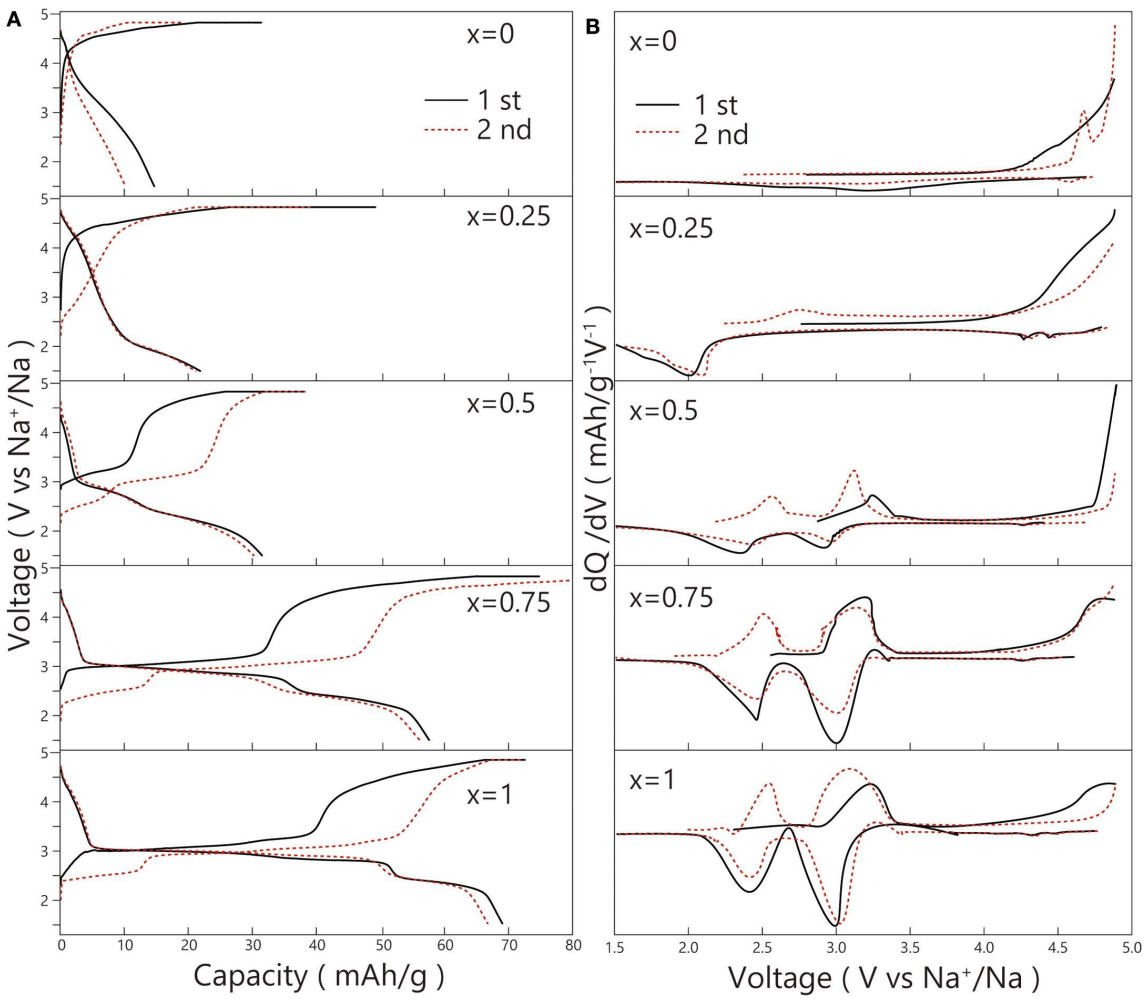

FIGURE 10 | (A) 1st and 2nd charge-discharge curves; **(B)** dQ/dV plots at 1st and 2nd cycles of the $Na_2Fe_xNi_{1-x}P_2O_7$ glass-ceramics.

Electrochemical Properties

The result of the first and second charge-discharge curves of the $Na_2Fe_xNi_{1-x}P_2O_7$ glass-ceramics is shown in **Figure 10A**. The initial discharge capacity of $Na_2Fe_xNi_{1-x}P_2O_7$ from $x = 0$ to 0.75 were 14.6, 21.8, 31.4, and 57.6 mAh/g. Each one was lower than that of $Na_2FeP_2O_7$ (68.7 mAh/g). It indicated that with the Fe

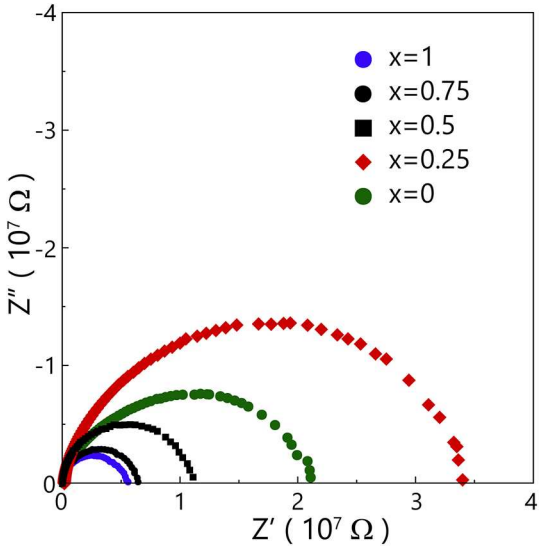

FIGURE 11 | Nyquist plots of heat-treated $Na_2Fe_xNi_{1-x}P_2O_7$ pellets at 220°C.

content increasing, the discharge capacity would be going up. In other words, it will be active with the Fe substitution increasing.

Furthermore, all the flat potential 3.0 or 2.5 V exhibited in the discharge process derived from the reduction of $Fe^{3+/2+}$ (Honma et al., 2012). However, the flat potential of $Ni^{3+/2+}$ did not exhibit in any composition. Even in the discharge process of $Na_2Fe_{0.25}Ni_{0.75}P_2O_7$, there was only a 2.0 V flat potential of $Fe^{3+/2+}$, suggesting the overvoltage caused by the inactive Ni existing.

To check the redox peaks in the process of charge and discharge, dQ/dV plots that transformed from the charge-discharge curves are shown in **Figure 10B**. In the 1st charge-discharge process of $Na_2NiP_2O_7$, there was none redox peak exhibited out, which showed the same result with Zhang et al. (2017). However, in the 2nd charge process, there was an oxidation peak of $Ni^{2+/3+}$ at about 4.6 V (Zhang et al., 2017) exhibited. In addition, in the discharge process of $Na_2Fe_{0.25}Ni_{0.75}P_2O_7$, despite there could be a weak electrolytic solution decomposition potential at about 4.3 V, it still exhibited the potential of $Ni^{3+/2+}$ at about 4.3 and 4.4 V. As a result, $Na_2Fe_xNi_{1-x}P_2O_7$ with the Fe substitution up to $x = 0.25$ will activate the $Ni^{3+/2+}$. However, in total, $Ni^{3+/2+}$ in the composition of $Na_2Fe_xNi_{1-x}P_2O_7$ exhibited inactivity.

To know the electrical conductivity of the positive electrode materials, we decided to measure their electrical resistance from 100 to 220°C. Considering the difference of crystallization behavior between bulk and powder, we chose to press the precursor glass powder as a pellet and then measured the electrical resistance of the pellets after heat-treatment under T_p. **Figure 11** shows Nyquist plots of crystallized $Na_2Fe_xNi_{1-x}P_2O_7$ pellets. The intersection of semicircle and horizontal axis determined the electrical resistance, so with the Fe substitution increased, the electrical resistance would be decreased. In other words, electrical conductivity would be increased. However, there was a result that the electrical resistance of $Na_2Fe_{0.25}Ni_{0.75}P_2O_7$ pellet was higher than that of the other components, which could confirm the same result exhibited in charge-discharge curves. Because of the exceptional electrical resistance exhibited in the composition of $Na_2Fe_{0.25}Ni_{0.75}P_2O_7$, so the reduction of $Fe^{3+/2+}$ would be alleviated. With the alleviating of $Fe^{3+/2+}$, the reduction peaks of $Ni^{3+/2+}$ which could be activated by the substituted Fe^{2+} exhibited out. However, the reduction peaks of $Ni^{3+/2+}$ disappeared at the composition $x = 0.5$ and 0.75. It may be owing to the active $Fe^{3+/2+}$ reduction reaction is dominant so the $Ni^{3+/2+}$ reduction reaction will be unavailable.

No matter which kind type of Ni-Fe substitution, it will increase the electric conductivity (Sanz et al., 2001) so that the $Ni^{2+,}$ which surrounds the substituted $Fe^{2+,}$ will be activated. Also, carbon-coatings will enhance the electrochemical behavior of the materials contained Fe (Wang and Sun, 2012), which can ensure a better charge-discharge cycle. However, the liquid electrolyte 1 mol/L EC: DEC [1:1 (vol%)]-$NaPF_6$ showed a decomposition potential at about 4.3 V. It could influence $Ni^{3+/2+}$ redox so that $Ni^{3+/2+}$ which has the higher potential (Zhang et al., 2017) did not exhibit out before 4.9 V. Because of the limitation of the liquid electrolyte, seeking the electrolyte with high decomposition potential is necessary.

CONCLUSION

In conclusion, the $Na_2Fe_xNi_{1-x}P_2O_7$ glasses were prepared by the melt-quenching method successfully. Moreover, the precursor $Na_2Fe_xNi_{1-x}P_2O_7$ glasses were confirmed that they contained a part of Fe^{3+}, which was oxidized from Fe^{2+}. $Na_{3.14}Ni_{2.18}(P_2O_7)_2$ crystal which was obtained from heat-treated $Na_2Fe_xNi_{1-x}P_2O_7$ glass-ceramics, mainly with type 1 Ni-Fe substitution. With the Fe substitution increasing in the $Na_{3.14}Ni_{2.18}(P_2O_7)_2$ crystal, it performed a higher activity. In the composition of $Na_2Fe_{0.25}Ni_{0.75}P_2O_7$, the reduction peaks of 4.3 and 4.4 V appeared in the discharge process. Although reversible charge-discharge reaction could not confirm due to interference with electrolyte oxidation, application to oxide all-solid-state batteries is expected to expand to batteries with higher energy density than sodium iron phosphate derived all-solid batteries.

DATA AVAILABILITY STATEMENT

The raw data supporting the conclusions of this article will be made available by the authors, without undue reservation, to any qualified researcher.

AUTHOR CONTRIBUTIONS

YJ demonstrated all experiments in the study. TH proposed glass-ceramic cathode for sodium ion battery. TK proposed the preparation of glass-ceramics and the analysis of surface crystallization.

FUNDING

This study was financially supported by JSPS KAKENHI Grant Number JP19K22046 and JP19H02428.

REFERENCES

Akatsuka, C., Honma, T., and Komatsu, T. (2018). Surface crystallization tendency of $Na_2FeP_2O_7$ glass. *J. Ceram. Soc. Jpn.* 126, 563–567. doi: 10.2109/jcersj2.18040

Angenault, J., Couturier, J. C., Quarton, M., and Robert, F. (1995). Structure of $Na_{3.12}Fe_{2.44}(P_2O_7)_2$. *Eur. J. Solid State Inorg. Chem.* 32, 335–343.

Barpanda, P., Liu, G., Ling C. D., Tamaru, M., Avdeev, M., Chung, S.-C., et al. (2013a). $Na_2FeP_2O_7$: a safe cathode for rechargeable sodium-ion batteries. *Chem. Mater.* 17, 3480–3487. doi: 10.1021/cm401657c

Barpanda, P., Lu, J., Ye, T., Kajiyama, M., Chung, S.-C., Yabuuchi, N., et al. (2013b). A layer-structured $Na_2CoP_2O_7$ pyrophosphate cathode for sodium-ion batteries. *RSC Adv.* 3, 3857–3860. doi: 10.1039/c3ra23026k

Barpanda, P., Oyama, G., Nishimura, S. I., Chung, S. C., and Yamada, A. (2014). A 3.8-V earth-abundant sodium battery electrode. *Nat. Commun.* 5:4358. doi: 10.1038/ncomms5358

Bianchini, F., Fjellvåg, H., and Vajeeston, P. (2018). A first-principle study of $NaMPO_4$ (M = Mn, Fe, Co, Ni) possible novel structures as cathode materials for sodium-ion batteries: structural and electrochemical characterisation. *Mater. Chem. Phys.* 219, 212–221. doi: 10.1016/j.matchemphys.2018.08.007

Chung, S.-Y., Bloking, J. T., and Chiang, Y. (2002). Electronically conductive phospho-olivines as lithium storage electrodes. *Nat. Mater.* 1, 123–128. doi: 10.1038/nmat732

Deubener, J., Allix, M., Davis, M. J., Duran, A., Höche, T., Honma, T., et al. (2018). Updated definition of glass-ceramics. *J. Non-Cryst. Solids* 501, 3–10. doi: 10.1016/j.jnoncrysol.2018.01.033

Ellis, B. L., Michael Makahnouk, W. R., Rowan-Weetaluktuk, W. N., Ryan, D. H., Nazar, L. F., Makahnouk, W. R. M., et al. (2010). Crystal structure and electrochemical properties of A_2MPO_4F fluorophosphates (A = Na, Li; M = Fe, Mn, Co, Ni). *Chem. Mater.* 22, 1059–1070. doi: 10.1021/cm902023h

Erragh, F., Boukhari, A., Abraham, F., and Elouadi, B. (2000). Study of the crystal structures of sodium magnesium and sodium nickel diphosphates. *J. Solid State Chem.* 152, 323–331. doi: 10.1006/jssc.2000.8651

Fang, Y., Liu, Q., Xiao, L., Ai, X., Yang, H., and Cao, Y. (2015). High-performance olivine $NaFePO_4$ microsphere cathode synthesized by aqueous electrochemical displacement method for sodium ion batteries. *ACS Appl. Mater. Interfaces* 7, 17977–17984. doi: 10.1021/acsami.5b04691

Finegan, D. P., Scheel, M., Robinson, J. B., Tjaden, B., Hunt, I., Mason, T. J., et al. (2015). Lithium-ion batteries during thermal runaway. *Nat. Commun.* 6:6924. doi: 10.1038/ncomms7924

Gutierrez, A., Benedek, N. A., and Manthiram, A. (2013). Crystal-chemical guide for understanding redox energy variations of $M^{2+/3+}$ couples in polyanion cathodes for lithium-ion batteries. *Chem. Mater.* 25, 4010–4016. doi: 10.1021/cm401949n

Hirose, K., Honma, T., Doi, Y., Hinatsu, Y., and Komatsu, T. (2008). Mössbauer analysis of Fe ion state in lithium iron phosphate glasses and their glass-ceramics with olivine-type $LiFePO_4$ crystals. *Solid State Commun.* 146, 273–277. doi: 10.1016/j.ssc.2008.02.013

Honma, T., Hirose, K., Komatsu, T., Sato, T., and Marukane, S. (2010). Fabrication of $LiFePO_4$/carbon composites by glass powder crystallization processing and their battery performance. *J. Non-Cryst. Solids* 356, 3032–3036. doi: 10.1016/j.jnoncrysol.2010.05.079

Honma, T., Ito, N., Togashi, T., Sato, A., and Komatsu, T. (2013). Triclinic $Na_{2-x}Fe_{1+x/2}P_2O_7$/C glass-ceramics with high current density performance for sodium ion battery. *J. Power Sources* 227, 31–34. doi: 10.1016/j.jpowsour.2012.11.030

Honma, T., Togashi, T., Ito, N., and Komatsu, T. (2012). Fabrication of $Na_2FeP_2O_7$ glass-ceramics for sodium ion battery. *J. Ceram. Soc. Jpn.* 120, 344–346. doi: 10.2109/jcersj2.120.344

Kim, H., Shakoor, R. A., Park, C., Lim, S. Y., Kim, J., and Jo, Y. N. (2013). $Na_2FeP_2O_7$ as a promising iron-based pyrophosphate cathode for sodium rechargeable batteries : a combined experimental and theoretical study. *Adv. Funct. Mater.* 23, 1147–1155. doi: 10.1002/adfm.201201589

Komatsu, T. (2015). Design and control of crystallization in oxide glasses. *J. Non-Cryst. Solids* 428, 156–175. doi: 10.1016/j.jnoncrysol.2015.08.017

Kundu, D., Talaie, E., Duffort, V., and Nazar, L. F. (2015). The emerging chemistry of sodium ion batteries for electrochemical energy storage. *Angew. Chemie Int. Ed.* 54, 3432–3448. doi: 10.1002/anie.201410376

Nagamine, K., Honma, T., and Komatsu, T. (2011). A fast synthesis of $Li_3V_2(PO_4)_3$ crystals via glass-ceramic processing and their battery performance. *J. Power Sources* 196, 9618–9624. doi: 10.1016/j.jpowsour.2011.06.094

Nagamine, K., Oh-Ishi, K., Honma, T., and Komatsu, T. (2012). Formation mechanism of $LiFePO_4$ in crystallization of lithium iron phosphate glass particles. *J. Ceram. Soc. Jpn.* 120, 193–198. doi: 10.2109/jcersj2.120.193

Nishi, Y. (2001). Lithium ion secondary batteries; past 10 years and the future. *J. Power Sources* 100, 101–106. doi: 10.1016/S0378-7753(01)00887-4

Nitta, N., Wu, F., Lee, J. T., and Yushin, G. (2015). Li-ion battery materials: present and future. *Mater. Today* 18, 252–264. doi: 10.1016/j.mattod.2014.10.040

Ong, S. P., Chevrier, V. L., Hautier, G., Jain, A., Moore, C., Kim, S., et al. (2011). Voltage, stability and diffusion barrier differences between sodium-ion and lithium-ion intercalation materials. *Energy Environ. Sci.* 4, 3680–3688. doi: 10.1039/c1ee01782a

Sanz, F., Parada, C., Rojo, J. M., and Ru, C. (2001). Synthesis, structural characterization, magnetic properties, and ionic conductivity of $Na_4M^{II}_3(PO_4)_2(P_2O_7)(M^{II})$Mn,Co,Ni). *Chem. Mater.* 3, 1334–1340. doi: 10.1021/cm001210d

Singh, P., Shiva, K., Celio, H., and Goodenough, J. B. (2015). Eldfellite, $NaFe(SO_4)_2$: an intercalation cathode host for low-cost Na-ion batteries. *Energy Environ. Sci.* 8, 3000–3005. doi: 10.1039/C5EE02274F

Slater, M. D., Kim, D., Lee, E., and Johnson, C. S. (2013). Sodium-ion batteries. *Adv. Funct. Mater.* 23, 947–958. doi: 10.1002/adfm.201200691

Spotnitz, R., and Franklin, J. (2003). Abuse behavior of high-power, lithium-ion cells. *J. Power Sources* 113, 81–100. doi: 10.1016/S0378-7753(02)00488-3

Tanabe, M., Honma, T., and Komatsu, T. (2018). Crystallization behavior and electrochemical properties of $Na_2Fe_yMn_{1-y}P_2O_7$ glass. *J. Non-Cryst. Solids* 501, 153–158. doi: 10.1016/j.jnoncrysol.2017.12.039

Wang, J., and Sun, X. (2012). Understanding and recent development of carbon coating on $LiFePO_4$ cathode materials for lithium-ion batteries. *Energy Environ. Sci.* 5, 5163–5185. doi: 10.1039/C1EE01263K

Wang, P. F., You, Y., Yin, Y. X., and Guo, Y. G. (2016). An O3-type $NaNi_{0.5}Mn_{0.5}O_2$ cathode for sodium-ion batteries with improved rate performance and cycling stability. *J. Mater. Chem. A* 4, 17660–17664. doi: 10.1039/C6TA07589D

Wang, Q., Ping, P., Zhao, X., Chu, G., Sun, J., and Chen, C. (2012). Thermal runaway caused fire and explosion of lithium ion battery. *J. Power Sources* 208, 210–224. doi: 10.1016/j.jpowsour.2012.02.038

Yabuuchi, N., Kajiyama, M., Iwatate, J., Nishikawa, H., Hitomi, S., Okuyama, R., et al. (2012). P2-type $Na_x[Fe_{1/2}Mn_{1/2}]O_2$ made from earth-abundant elements for rechargeable Na batteries. *Nat. Mater.* 11, 512–517. doi: 10.1038/nmat3309

Yamauchi, H., Ikejiri, J., Sato, F., Oshita, H., Honma, T., and Komatsu, T. (2019). Pressureless all-solid-state sodium-ion battery consisting of sodium iron pyrophosphate glass-ceramic cathode and β''-alumina solid electrolyte composite. *J. Am. Ceram. Soc.* 102, 6658–6667. doi: 10.1111/jace.16607

Zhang, H., Hasa, I., Buchholz, D., Qin, B., Geiger, D., Jeong, S., et al. (2017). Exploring the Ni redox activity in polyanionic compounds as conceivable high potential cathodes for Na rechargeable batteries. *NPG Asia Mater.* 9:e370. doi: 10.1038/am.2017.41

Conflict of Interest: The authors declare that the research was conducted in the absence of any commercial or financial relationships that could be construed as a potential conflict of interest.